Title	Error calibration of five-axis machine tools by on-machine measurement system using a laser displacement sensor
Author(s)	NAGAI, Yuu; IBARAKI, Soichi; NISHIKAWA, Shizuo
Citation	Journal of Advanced Mechanical Design, Systems, and Manufacturing (2014), 8(4)
Issue Date	2014-10-31
URL	http://hdl.handle.net/2433/192480
Right	© 2014 The Japan Society of Mechanical Engineers
Type	Journal Article
Textversion	author

JSME Journal Template

Error calibration of five-axis machine tools by on-machine measurement system using a laser displacement sensor

Yuu NAGAI*, Soichi IBARAKI* and Shizuo NISHIKAWA**
* Department of Micro Engineering, Graduate School of Engineering, Kyoto University,
Kyotodaigaku Katsura, Nishikyo-ku, Kyoto 615-8540, Japan
E-mail: ibaraki@prec.kyoto-u.ac.jp
**Department of Mechanical Engineering, Kikai University
632 Idono, Yamatokoriyama, Nara, 639-1183, Japan

Received 28 February 2014

Abstract
An on-machine measurement system to measure the workpiece's geometry or dimension plays an important role in manufacturing processes. A laser displacement sensor recently attracts more attention which enables on-machine high-speed continuous scanning measurement. We developed an on-machine measurement system using a triangulation-based laser displacement sensor for five-axis machine tools. By driving the machine's rotary axes to tilt or rotate the workpiece, the object's geometry can be measured from all the directions in the three-dimensional space without being detached from a machine table. In such a measurement, location errors and error motions of the machine's rotary axes clearly become major contributors for the measurement uncertainty. To identify location errors of rotary axes by using the on-machine laser measurement system itself, this paper presents its application to the R-test, where the three-dimensional displacement of a precision sphere, attached to a rotary table, is measured in the machine tool coordinate system. In the present laser measurement system, the position and the orientation of the laser displacement sensor must be calibrated in advance by using the motion of the machine's rotary axes. The location errors of rotary axes cause their identification error. Unlike the conventional R-test, where the sphere's displacement is measured by three contact-type displacement sensors, the formulation to identify location errors must consider the influence of this calibration error. Experimental demonstration is presented.
Keywords : five-axis machine tool, on-machine measurement, laser displacement sensor, triangulation, location errors, R-test.

1. Introduction

Nowadays, the machining of high precision products is demanded in various manufacturing fields. On-machine measurement, integrating the measuring process into the machining process, can contribute to the improvement of machining accuracy and efficiency by either pre-machining measurement of workpiece setup or post-machining measurement for the rectification of the machined workpiece.

As an instrument for on-machine measurement, a laser displacement sensor recently attracts more attention. Compared with a touch-triggered probe, which is more common in today's market, a laser displacement sensor has a strong advantage in its capability to perform high-speed continuous scanning measurement without damaging the object's surface. Furthermore, as is illustrated in Fig. 1, when the object is measured with driving the machine tool's rotary axes, its three-dimensional geometry is measured from all the directions without dismounting from a machine table.

In such a measurement, error motions of the machine tool itself are clearly one of major contributors for the measurement uncertainties. In particular, the influence of rotary axes' error motions become larger as the measuring point is further from the rotary axis centerline, and thus they are often dominating contributors on the measurement uncertainty. Location errors (ISO230-7, 2006) associated with rotary axes, such as the squareness error between a rotary axis average line (ISO230-7, 2006) and a linear axis, can be seen as the most fundamental errors in 5-axis

Paper No.xx-xxxx
[DOI: 10.1299/mej.2014smm000x]

kinematics.

This paper presents a method to identify the location errors of rotary axes by using the present on-machine laser measurement system. Since many latest commercial CNCs have the functionality of compensating for rotary axes error motions, this identification can potentially improve the measurement accuracy.

The present identification scheme of rotary axis location errors is essentially the same as the R-test. The R-test was first presented by Weikert (Weikert, 2004). The static R-test procedure to identify all the rotary axis location errors was first presented in (Bringmann and Knapp, 2006). In the R-test procedure, a precision sphere is attached to a machine spindle. Three (or four) contact-type linear displacement sensors are attached on a fixture that is fixed on a machine table. As a rotary table rotates, the sphere is moved by linear axes such that its displacement to the rotary table becomes nominally zero. Its actual three-dimensional displacement is measured by three sensors. Analogous calibration schemes using a touch-triggered probe to statically measure the sphere position are commercially available from several vendors (Ibaraki and Ota, 2014).

In the proposed scheme, the three-dimensional position of a sphere, attached to the machine's rotary table, is measured by using the on-machine laser measurement system. In the present laser measurement system, the position and the orientation of the laser displacement sensor must be calibrated in advance by using the motion of the machine's rotary axes. The location errors of rotary axes cause their identification error. The formulation to identify location errors is significantly different from the conventional R-test, in that the influence of this calibration error must be taken into consideration. This formulation is one of this paper's original contributions.

The experimental case study will be presented.

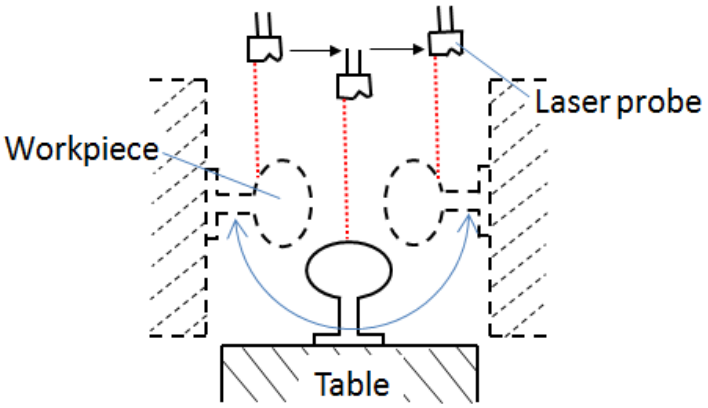

Fig. 1: On-machine measurement with continuously tilting the workpiece.

2. On-machine 5-axis laser measuring system

2.1 Machine configuration and kinematic model

This paper considers the 5-axis machine configuration with a tilting rotary table (B- and C-axes) depicted in Fig. 2. It is important to note that this paper's basic idea can be extended to any configurations of 5-axis machine tools.

ISO 230-7:2006 defines the axis average line as "a straight line segment located with respect to the reference coordinate axes representing the mean location of the axis of rotation." For machine configuration illustrated in Fig. 2, total eight geometric error parameters, shown in Table 1, are sufficient to characterize the position and the orientation of B- and C-axis average lines (Inazaki, et al., 1997). These parameters are called "location errors" in ISO 230-7 (2006).

The kinematic model of this 5-axis machine tool is based on the coordinate transformation between the workpiece coordinate system and the machine coordinate system. Here, the workpiece coordinate system is defined as the coordinate system attached to the rotary table, driven by B- and C-axis with location errors shown in Table 1. The origin of the machine coordinate system is set at the nominal intersection of B- and C-axis. The homogeneous transformation matrix (HTM) from the workpiece coordinate system to the machine coordinate system is given by:

$$ {}^{r}T_{w}\left(B_i, C_j\right) = D_x(\delta x_{BY}) D_y(\delta y_{BY}) D_z(\delta z_{BY}) D_a(\alpha_{BY}) D_b(\beta_{BY}) D_c(\gamma_{BY}) D_b(-B_i) $$

[DOI: 10.1299/mej.2014smm000x]

$$D_x(\delta x_{CB})D_a(\alpha_{CB})D_c(-C_j) \tag{1}$$

where $D_x(x)$, $D_y(y)$, and $D_z(z)$ $\in \mathbf{R}^{4\times4}$ is the HTM for linear motions in X-, Y-, and Z-directions. $D_a(a)$, $D_b(b)$, and $D_c(c)$ represent the HTM of the rotation around X-, Y-, and Z-axes. See e.g. [2] for the formulation of HTMs. B_i and C_j is angular command of B- and C-axis. Hence, the point in workpiece coordinate system, denoted by ${}^w p \in \mathbf{R}^3$, is transformed into the machine coordinate system by:

$$\begin{bmatrix} {}^r p \\ 1 \end{bmatrix} = {}^r T_w(B_i, C_j) \cdot \begin{bmatrix} {}^w p \\ 1 \end{bmatrix} \tag{2}$$

The superscripts w and r respectively denote a vector represented in the workpiece coordinate system and the machine coordinate system.

This study assumes that the error motions of linear axes are pre-calibrated, and they are sufficiently smaller than those of the rotary axes.

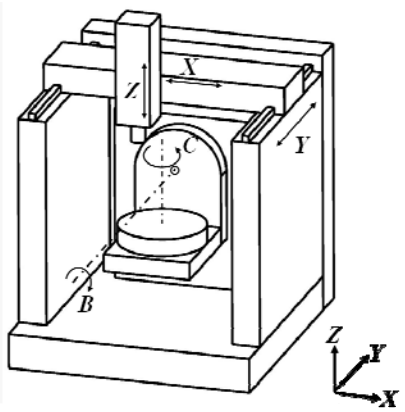

Fig. 2: The configuration of a 5-axis machine tool.

Symbol in (Inazaki, 1997)	Symbol in (ISO230-1, 2012)	Description
δx_{BV}	E_{X0B}	Position error of B-axis average line in X direction
δy_{BV}	E_{Y0B}	Position error of C-axis average line in Y direction
δz_{BV}	E_{Z0B}	Position error of B-axis average line in X direction
δx_{CB}	$E_{X0C} - E_{X0B}$	Linear offset of C-axis from B-axis in X direction
α_{BV}	E_{A0B}	Squareness error of B- to Z-axis
β_{BV}	E_{B0B}	Angular positioning error of B-axis at $B = 0^\circ$
γ_{BV}	E_{C0B}	Squareness error of B- to X-axis
α_{CB}	$E_{A0C} - E_{A0B}$	Squareness error of C- to B-axis

Table 1: Geometric error parameters of rotary axis average lines for the machine configuration in Fig.2

2.2 Measurement principle of the developed 5-axis laser measurement system

In this paper, we employ a triangulation-based laser displacement sensor using the diffuse reflection. See e.g. (Kimura, et al., 2012a) for this sensor's measurement principle. It has a strong advantage in measuring tilted or spherical surface. According to our previous study (Kimura, et al., 2012b), depending on the object's surface roughness, it can measure the plane tilted from the sensor's sensitive direction by up to 40°. This robustness is valuable for on-machine measurement, where the uncertainty in the pre-knowledge for workpiece's geometry or position may be significantly large.

In this on-machine measurement system, X, Y, and Z positions are measured by each axis' linear encoder,

[DOI: 10.1299/mej.2014smm000x]

synchronously with the laser displacement, $d(k)$, where k is the sampled number. Figure 3 shows the schematic drawing of this measuring system, where the laser displacement sensor is mounted on the machine spindle. The intersection of the spindle axis average line and the spindle gauge line is called *the spindle datum point* in this paper. As mentioned above, we assume that error motions of the linear axes are negligible, and thus X, Y, and Z positions measured by linear encoders represent the position of the spindle datum point, ${}^r p_c(k) \in \mathbf{R}^3$, in the machine coordinate system. *The light spot position*, i.e. the intersection of the laser beam axis and the object surface, denoted by ${}^r p(k) \in \mathbf{R}^3$ is calculated by:

$$ {}^r p(k) = {}^r p_c(k) - \vec{l} + d(k) \cdot \vec{t} \tag{3}$$

where *the direction vector of laser beam*, $\vec{t} \in \mathbf{R}^3$, is a unit vector of the sensor's sensitive direction. $\vec{l} \in \mathbf{R}^3$ represents *the sensor's zero position vector*, which is a vector from the sensor's zero point to the spindle datum point. The sensor's zero point is the point on the laser beam axis with $d(k) = 0$. The calibration of $\vec{t}$ and $\vec{l}$ will be discussed in Section 3. To observe a workpiece's surface profile, the measured light spot position in the machine coordinate system should be converted to the nominal workpiece coordinate system. Here *the nominal workpiece coordinate system* is defined by rotating the machine coordinate system by B_i and C_j, command angular positions of B- and C-axis. This transformation is given by:

$$\begin{bmatrix} {}^w p^*(B_i, C_j) \\ 1 \end{bmatrix} = \left({}^r T_w^*(B_i, C_j) \right)^{-1} \cdot \begin{bmatrix} {}^r p(B_i, C_j) \\ 1 \end{bmatrix} \tag{4}$$

$$ {}^r T_w^*(B_i, C_j) = D_b(-B_i) D_c(-C_j)$$

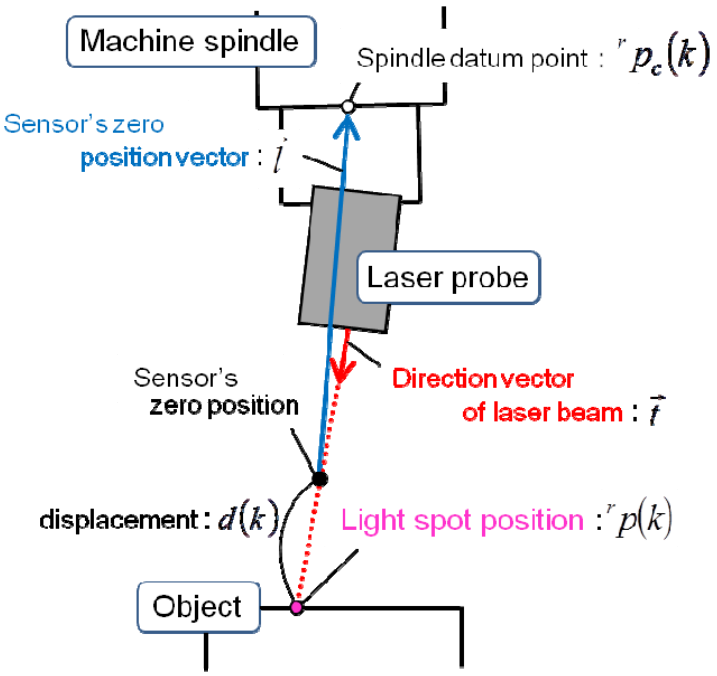

Fig. 3: Laser displacement sensor setup to measure the light spot position

3. Calibration of laser beam direction vector and zero position vector

3.1 Outline

As shown by Eq. (3), to calculate the light spot position, ${}^r p(k)$, the direction vector of laser beam. $\vec{t}$. and the sensor's zero position vector, $\vec{l}$, must be pre-calibrated. Such a pre-calibration is also needed for touch-triggered probes. A calibration method for contact-type sensors like a touch-triggered probe generally requires the physical contact of the probe and a displacement sensor. However, since a laser displacement sensor does not have a contactable

[DOI: 10.1299/mej.2014smm000x]

probe, this pre-calibration is more difficult. In this paper, $\vec{t}$ and $\vec{l}$ are calibrated in reference to the machine tool's motion.

A precision sphere, of sufficiently high geometric accuracy, is fixed on the machine table. As illustrated in Fig. 4, the sensor is moved along cross-shaped circular pass. This operation is hereafter called *the scanning operation of a sphere*. From the light position, ${}^{r}p(k)$, given by Eq. (3) with the initial $\vec{t}$ and $\vec{l}$, the sphere's center, ${}^{r}q \in \mathbf{R}^3$, is calculated by solving the following minimization problem:

$$\min_{{}^{r}q} \sum_{k} \left\{ \left\| {}^{r}p(k) - {}^{r}q \right\| - R \right\}^2 \tag{5}$$

where $R \in \mathbf{R}$ is the sphere's radius, and $\|*\|$ denotes the 2-norm of a vector. Throughout this paper, the notation ${}^{*}p$ represents the light spot position, and ${}^{*}q$ represents the point calculated from a set of measured light spots.

3.2 Calibration of the laser beam direction

The direction vector of laser beam, $\vec{t}$, is identified as the parallelism error of the sensor's sensitive direction and the machine's Z-axis reference straight line. As illustrated in Fig. 5, first, the sensor is positioned where its zero position is approximately on the sphere's surface. At this position, the scanning procedure in the previous subsection is performed. Then, repeat the same scanning procedure at different two Z positions. Using the spindle datum position ${}^{r}p_c(k)$ and laser displacement $d(k)$ obtained by these processes, we can estimate the laser beam direction, $\vec{t}$ and the sphere's center, ${}^{r}q$, by solving:

$$\min_{\vec{t},{}^{r}q} \sum_{k} \left\{ \left\| {}^{r}p_c(k) + d(k)\cdot\vec{t} - {}^{r}q \right\| - R \right\}^2 \tag{6}$$

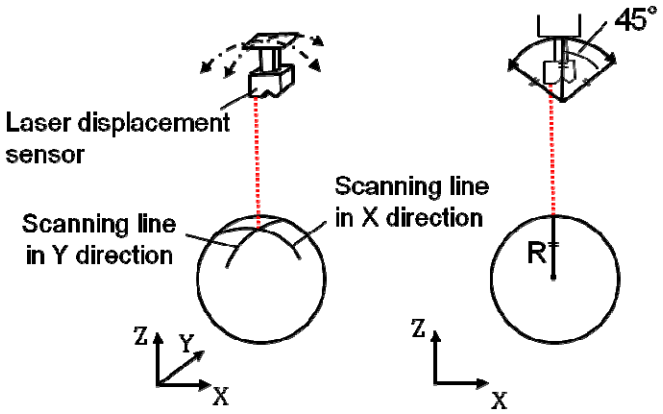

Fig. 4: Scanning operation of sphere to measure its center position.

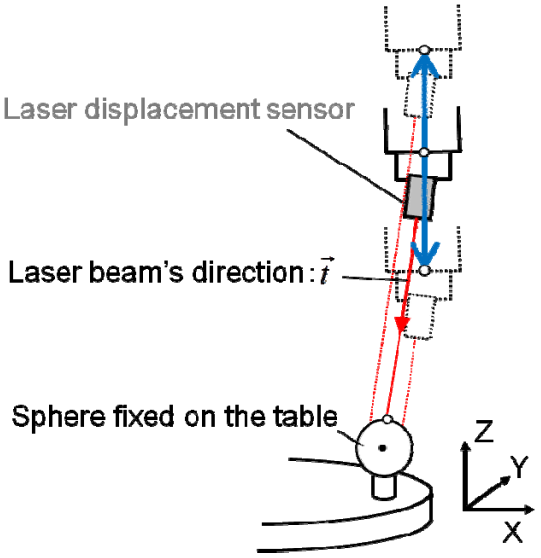

Fig. 5: Calibration procedure of the laser beam direction

3.3 Calibration of the sensor's zero position vector

The sensor's zero position vector, $\vec{l}$, is estimated based on the nominal position of the machine's each rotary axis average line. The nominal position of rotary axis average line in the machine coordinate system, i.e. the encoder position of the spindle datum point when it is on the rotary axis average line, is typically pre-calibrated by a machine tool builder (or a user) and saved in the CNC system.

Figure 6 illustrates this calibration procedure with B-axis motion, as an example. First, at B_1=0°, perform the scanning procedure in Section 3.1 and calculate the sphere's center position ${}^{r}q(B_1)$ by Eq. (3) and Eq. (5) with $\vec{l} = [0,0,0]^T$. At various B angles, B_i (i=2～N_b), repeat this process to get the sphere's position ${}^{r}q(B_i)$. Then, the center position of trajectory of ${}^{r}q(B_i)$, denoted by ${}^{r}o_b \in \mathbf{R}^3$, is calculated by best-fitting to a circle. The sensor's zero

[DOI: 10.1299/mej.2014smm000x]

position vector $\vec{l}$ is given by:

$$\left[\vec{l}(1),\vec{l}(3)\right]^T = \left[{}^r o_b(1),{}^r o_b(3)\right]^T - \left[{}^r o_b^*(1),{}^r o_b^*(3)\right]^T \tag{7}$$

where ${}^r o_b^* \in \mathbf{R}^3$ is the nominal position of B-axis average line. According to the machine coordinate system's definition, $[\,{}^r o_b^*(1),\ {}^r o_b^*(3)\,] = [0,0]^T$.

By an analogous procedure for C-axis, we can calculate $[\vec{l}(1),\vec{l}(2)]$. When there exist rotary axes' geometric errors, the identified $\vec{l}(1)$ by the two procedures may not be the same. In this paper, we adopt the result from the procedure for C-axis as $\vec{l}(1)$.

This calibration is based on the assumption that there is no calibration error in the nominal position, and no radial error motions, of B- and C- axes. When this assumption is not met, the sensor's zero position vector $\vec{l}$ is miscalibrated. This will be discussed in the next subsection.

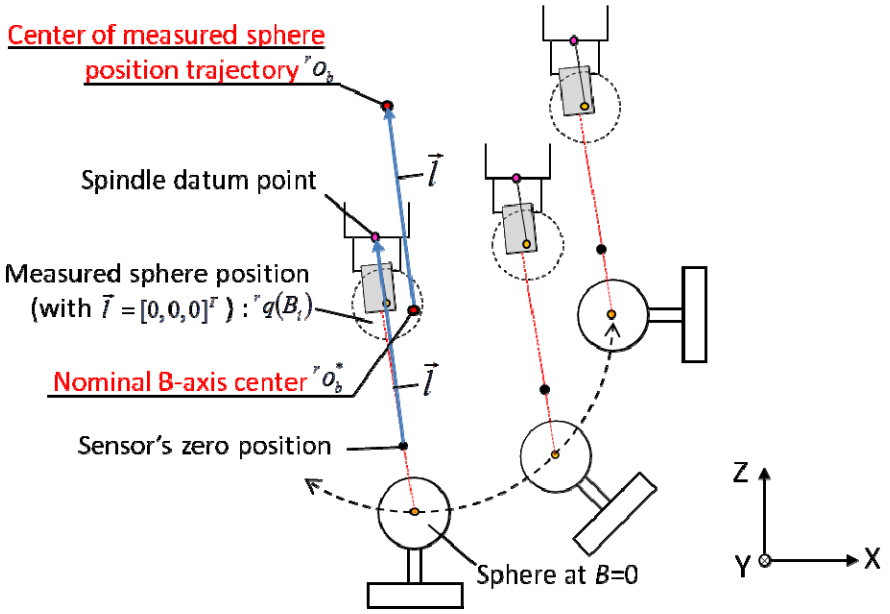

Fig. 6: Calibration procedure of sensor's zero position vector

3.4 Calibration error of the sensor's zero position vector

The geometric errors of rotary axes cause miscalibration of the sensor's zero position vector, $\vec{l}$. This subsection formulates its calibration error caused by location errors in Table 1.

In the calibration procedure presented in Section 3.3, the rotation center, ${}^r o_b$, is calculated by curve-fitting the trajectory of measured sphere positions, ${}^r q(B_i)$. Here, to simplify the formulation, ${}^r o_b$ is calculated from the sphere position at B =0° and 180°, respectively denoted by ${}^r q(0,0)$ and ${}^r q(180,0)$, i.e.

$${}^r o_b = \left\{{}^r q(0,0) + {}^r q(180,0)\right\}/2 \tag{8}$$

When $\Delta X, \Delta Y, \Delta Z, \Delta A, \Delta B,$ and ΔC are sufficiently small, the following approximation generally holds:

$$D_x(\Delta X)D_y(\Delta Y)D_z(\Delta Z)D_a(\Delta A)D_b(\Delta B)D_c(\Delta C) \approx \begin{bmatrix} 1 & -\Delta C & \Delta B & \Delta X \\ \Delta C & 1 & -\Delta A & \Delta Y \\ -\Delta B & \Delta A & 1 & \Delta Z \\ 0 & 0 & 0 & 1 \end{bmatrix} \tag{9}$$

Using this approximation, under the assumption that all location errors are sufficiently small, ${}^r q(0,0)$ is formulated by Eq. (1) and (2) as:

[DOI: 10.1299/mej.2014smm000x]

$$\begin{bmatrix} {}^{r}q(0,0) \\ 1 \end{bmatrix} = {}^{r}T_{w}(0,0)\cdot\begin{bmatrix} {}^{w}q^{*} \\ 1 \end{bmatrix} \approx \begin{bmatrix} 1 & -\gamma_{BY} & \beta_{BY} & \delta x_{BY}+\delta x_{CB} \\ \gamma_{BY} & 1 & -\alpha_{BY}-\alpha_{CB} & \delta y_{BY} \\ -\beta_{BY} & \alpha_{BY}+\alpha_{CB} & 1 & \delta z_{BY} \\ 0 & 0 & 0 & 1 \end{bmatrix}\cdot\begin{bmatrix} {}^{w}q^{*} \\ 1 \end{bmatrix} \tag{10}$$

where ${}^{w}q_0^* = [{}^{w}q_0^*(1), {}^{w}q_0^*(2), {}^{w}q_0^*(3)]^T$ represents the sphere position in the workpiece coordinate system. ${}^{r}q(180,0)$ can be derived similarly. Then, Eq. (8) gives:

$${}^{r}o_b \approx \begin{bmatrix} -\gamma_{BY}\,{}^{w}q_0^*(2)+\delta x_{BY} \\ {}^{w}q_0^*(2)-\alpha_{CB}\,{}^{w}q_0^*(3)+\delta y_{BY} \\ \alpha_{BY}\,{}^{w}q_0^*(2)+\delta z_{BY} \end{bmatrix} \tag{11}$$

By substituting Eq. (11) into Eq. (7), the calibration error e_b^2 is given by:

$$\vec{e_b} = [\vec{l}(1), \vec{l}(3)]^T - [\vec{l}^*(1), \vec{l}^*(3)]^T \approx \begin{bmatrix} -\gamma_{BY}\,{}^{w}q_0^*(2)+\delta x_{BY} \\ \alpha_{BY}\,{}^{w}q_0^*(2)+\delta z_{BY} \end{bmatrix} \tag{12}$$

As was described in Section 3.3, X- and Y-components of $\vec{l}$ are identified by the center position of C-rotation. Their identification error can be formulated similarly:

$$\vec{e_c} = [\vec{l}(1), \vec{l}(2)]^T - [\vec{l}^*(1), \vec{l}^*(2)]^T \approx \begin{bmatrix} \beta_{BY}\,{}^{w}q_0^*(3)+\delta x_{BY}+\delta x_{CB} \\ -(\alpha_{BY}+\alpha_{CB})\,{}^{w}q_0^*(3)+\delta y_{BY} \end{bmatrix} \tag{13}$$

When the X-component of $\vec{l}$ is taken from Eq. (13), as was mentioned in Section 3.3, the influence of location errors on the identification of $\vec{l}$ is summarized as:

$$\vec{e} = \vec{l} - \vec{l}^* = \begin{bmatrix} \beta_{BY}\,{}^{w}q_0^*(3)+\delta x_{BY}+\delta x_{CB} \\ -(\alpha_{BY}+\alpha_{CB})\,{}^{w}q_0^*(3)+\delta y_{BY} \\ \alpha_{BY}\,{}^{w}q_0^*(2)+\delta z_{BY} \end{bmatrix} \tag{14}$$

When the zero position vector, $\vec{l}$, contains this calibration error, the measured position ${}^{r}\hat{p}(k) \in \mathbf{R}^3$ is given by following equation using Eq. (3).

$$\begin{aligned} {}^{r}\hat{p}(k) &= {}^{r}p_c(k) - (\vec{l}^* + \vec{e}) + d(k)\cdot\vec{t} \\ &= ({}^{r}p_c(k) - \vec{l}^* + d(k)\cdot\vec{t}) - \vec{e} = {}^{r}p(k) - \vec{e} \end{aligned} \tag{15}$$

where ${}^{r}p(k)$ represents the ideal measured position, with the true $\vec{l}^*$. Namely, the calibration error of $\vec{l}$ leads to the measured position's shift by $-\vec{e}$.

Suppose that a point is located at ${}^{w}p^* \in \mathbf{R}^3$ in the workpiece coordinate system. When B- and C-axis are indexed at B_i and C_j, the point is mapped in the machine coordinate system to ${}^{r}p(B_i, C_j)$ given in Eq. (2). The measured position, denoted by ${}^{r}\hat{p}(B_i, C_j)$, is influenced by the miscalibration error above, $\vec{e}$, and is given by following equation.

$$\begin{bmatrix} {}^{r}\hat{p}(B_i, C_j) \\ 1 \end{bmatrix} = D_x(-\beta_{BY}\,{}^{w}q_0^*(3) - \delta x_{CB})D_y((\alpha_{BY}+\alpha_{CB})\,{}^{w}q_0^*(3))D_z(-\alpha_{BY}\,{}^{w}q_0^*(2)) \\ D_a(\alpha_{BY})D_b(\beta_{BY})D_c(\lambda_{BY})D_b(-B_i)D_x(\delta x_{CB})D_a(\alpha_{CB})D_c(-C_j)\begin{bmatrix} {}^{w}p^* \\ 1 \end{bmatrix} \tag{16}$$

See (Kimura, et al. (2012a)) for more detailed derivation of this formulation. An important observation here is that Eq. (16) does not include position errors of B- or C-axis, $\delta x_{BY}, \delta y_{BY}, \delta z_{BY}$. This means that the present laser measurement system can perform accurate position measurement regardless of the three parameters.

4. Identification of location errors of rotary axes

[DOI: 10.1299/mej.2014smm000x]

The objective of this paper is to present a method to identify location errors of the machine tool's rotary axes, shown in Table 1, which are one of major contributors for the measurement uncertainty of the present 5-axis on-machine measurement system. This measurement procedure can be done by using the present laser measurement system itself. First, the measuring procedure will be presented in Section 4.1. The identification of location errors is based on the kinematic relationship between the measured sphere positions and the machine tool's location errors. The model presented in Section 3.4 is indispensable to describe this relationship. An identification algorithm will be presented in Section 4.2. Then, the experimental result will be presented to evaluate the validity of this method in the last subsection.

4.1 Measuring procedure

A precision sphere is fixed on the work table. As illustrated in Fig. 7, the work table is indexed at combination of given B- and C-angular positions, B_i (i=1～N_b), C_j (j=1～N_c). Measurement poses, B_i and C_j, must be distributed over the entire workspace of each rotary axis. At each angle, perform the scanning operation illustrated in Fig. 4 to measure the sphere's position.

4.2 Algorithm of location errors' identification

As shown in Section 3.4, the position errors of B- or C-axis average line, $\delta x_{BY}, \delta y_{BY}, \delta z_{BY}$, have no influence on the measurement. Thus, we can identify only five location errors, $W = [\alpha_{BY}, \beta_{BY}, \gamma_{BY}, \delta x_{CB}, \alpha_{CB}]^T$.

The kinematic relationship between the measured sphere's position at each measurement pose, ${}^r\hat{q}(B_i, C_j)$, and location errors, W, is described by Eq. (16). The sphere's nominal position, ${}^r q^*(B_i, C_j)$, is given in reference to the measured position at B=0°, C=0° as:

$$\begin{bmatrix} {}^r q^*(B_i, C_j) \\ 1 \end{bmatrix} = D_b(-B_i) D_b(-C_j) \begin{bmatrix} {}^r\hat{q}(0,0) \\ 1 \end{bmatrix} \tag{17}$$

The relative displacement of the measured position from the nominal position is denoted by ${}^r d(B_i, C_j)$. Then, the Jacobian matrix, $\partial({}^r d)/\partial W$, can be analytically formulated by Eqs. (2), (16) and (17). For example:

$$\frac{\partial d_x(B_i, C_j)}{\partial \alpha_{BY}} = \left\{ {}^r q^*(0,0)_y - {}^r q^*(B_i, C_j)_y \cdot \cos C_j \right\} \sin B_i + \left\{ {}^r q^*(0,0)_z \cdot \cos B_i - {}^r q^*(B_i, C_j)_z \right\} \sin C_j \tag{18}$$

where, ${}^r q^*(0,0)_y$ for example, denotes the y-component of the vector ${}^r q^*(0,0)$.

From the measured sphere's position, error parameters are identified by the least-squares method to solve the following problem.

$$\begin{aligned} &\min_W \sum_{i,j} \left\| {}^r d(B_i, C_j) - \frac{\partial {}^r d(B_i, C_j)}{\partial W} W \right\|^2 \\ &{}^r d(B_i, C_j) = {}^r\hat{q}(B_i, C_j) - {}^r q^*(B_i, C_j) \end{aligned} \tag{19}$$

4.3 Experimental evaluation of measurement accuracy of sphere displacement

Major specifications of the laser displacement sensor used in the experiments are shown in Table 2. Generally, the measurement uncertainty of a triangulation-based laser displacement sensor can be strongly dependent on the inclination of the target surface. When a spherical surface is scanned, the target surface within the laser spot would be inevitably tilted. The sensor's catalog does not clearly state the measurement uncertainty induced by the inclination of the target surface. Our previous study (Kimura, et al., 2012b) experimentally investigated this uncertainty for a sensor of the same measuring principle. Compared to a triangulation-based laser displacement sensor using the specular reflection, the one using the diffuse reflection (employed in our study) is significantly less sensitive to the inclination of the target surface. This subsection presents the experimental investigation of this sensor's uncertainty in measuring a

[DOI: 10.1299/mej.2014smm000x]

sphere's displacement.

Major specifications of the machine tool are shown in Table 3. Specifications of the precision sphere are shown in Table 4. For a diffuse reflection-based laser displacement sensor, it is known that the specular reflection of laser beam directly reaching the sensor's CCD array often causes the measurement error (Kimura, et al., 2012b). To mitigate this influence, an anti-reflective coating is applied to the sphere's surface.

The precision sphere is installed on the work table. The sensor's initial position is set such that its zero position is approximately on the spherical surface and the sphere's center is on the laser beam direction. Then, perform the scanning procedure in Fig. 4 to measure the sphere's initial position. The sensor is moved to the each vertex of a 0.2mm^3 cube shown in Fig. 8. At each vertex, repeat the scanning procedure and measure the sphere's position.

When the machine tool's positioning error is sufficiently small compared to the moving distance (0.2 mm), an error of the measured sphere displacement from its command position can be regarded as a measurement error of the present measurement system. Figure 8 shows the spindle's commanded and measured position, respectively denoted by black points and white circles.

From Fig. 8, the maximum error is about 1.4 μm. The machine tool's positioning error within this 0.2mm^3 cube was not accurately calibrated. According to the manufacture's pre-calibration or our own measurement, however, it can be reasonably assumed that it is not significantly smaller than 1.4 μm (the machine's positioning resolution is 1 μm).Therefore, it is concluded that the sphere's displacement measurement meets the required precision.

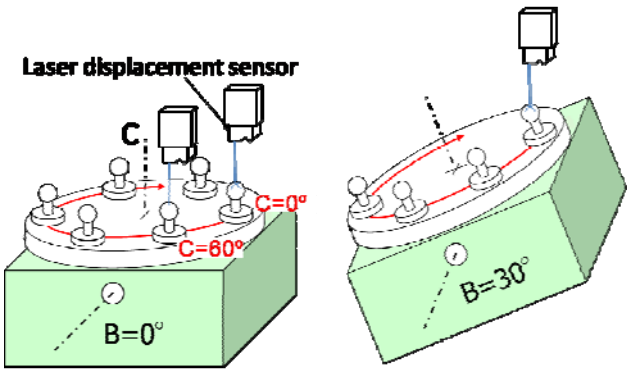

Fig. 7: R-test procedure by using the laser displacement system; at $B=0^{\circ}$ and at various B angles.

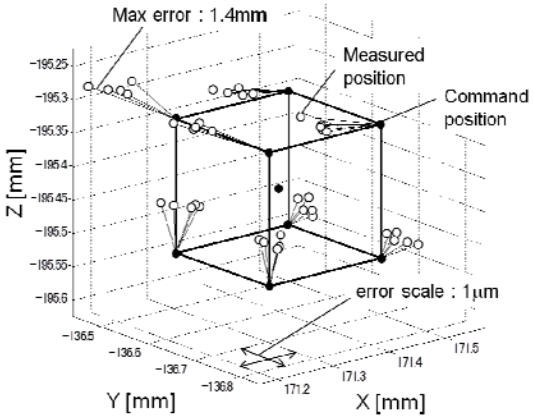

Fig. 8: The result of measurement of the sphere's relative displacement.

Table 2: Major specifications of the laser displacement sensor

Reference distance	50mm
Measurement range	20mm(±10mm)
Spot diameter at reference distance	50μm
Sampling frequency	1000Hz
Linearity	±0.02% of F.S. F.S.=20 mm
Repeatability	0.025 μm

Table 3: Major specifications of the machine tool

Axis	X	Y	Z	B	C
Stroke	420 mm	210 mm	400 mm	-180° ～160°	360°
Drives	Servo motor + ball screw			Direct drive	
Table Size	ϕ 250 mm				

Table 4 Major specifications of the precision sphere

Material	Tungsten-carbide
Diameter	20.000 mm ±2.5 μm
Roundness (in three planes)	0.13 μm
Surface roughness	0.025 μm (GR10)

[DOI: 10.1299/mej.2014smm000x]

5. Case study

This section demonstrates the case study of the identification method presented in Section 4.

5.1 Experimental setup

The same machine tool (Table 3) and the sensor (Table 2) were used. In this test, commanded B and C angular positions are given by:

$B_i = -90^\circ, -60^\circ, \ldots, 90^\circ$ (i=1,…,7)

$C_j = 0^\circ, 60^\circ, \ldots, 300^\circ$ (j=1,…,6)

Total 7×6=42 points are measured.

5.2 Measurement result

Figure 9 shows measured sphere's position, ${}^r\hat{q}(B_i, C_j)$, with full C-rotation (Cj =0°,…300°) at Bi =−90°,0°, and 90°, projected onto the XZ plane. In these plots, the command positions of the sphere, represented by a black painted circle, are plotted with the axis scale. The measured sphere positions, represented by a blue circle, are plotted with the error from its command position magnified 10,000 times. The "error scale" in Fig. 9(b) shows the scale for the error between command and measured sphere positions. Table 5 shows identified value of rotary axis' location errors. Using these parameters, the sphere's position is simulated by the kinematic model, Eq. (16), and its trajectory is represented by the triangles in Fig. 9. "Table" indicates the approximate position and orientation of rotary table.

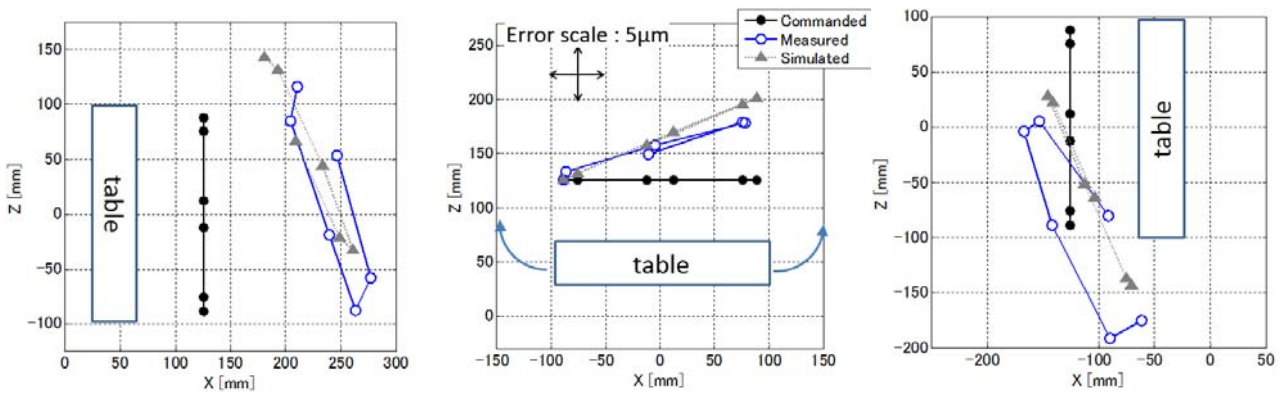

(a) At B = −90° (b) At B = 0° (c) At B = 90°

Fig. 9: Sphere positions measured with C-rotation at B = −90°,0°, and 90°, projected on XZ plane

Table 5: Identified parameters of location error.

α_{BY}	-3.5 μrad
β_{BY}	-42 μrad
γ_{BY}	-3.5 μrad
δx_{CB}	-1.0 μm
α_{CB}	5.2 μrad

5.3 Observation

From Fig. 9, many observations can be made to intuitively understand error motions of rotary axes. For example:

- In Fig. 9 (b), the trajectory of measured sphere's position (denoted by circles) are tilted to the left. This shows the squareness error of the C-axis average line to X-axis at B = 0°, which is parameterized by β_{BY} in Table 5. This can be observed at all B angular positions.
- The trajectory of commanded positions is projected as a straight line on the XZ plane in Fig. 9. The trajectories of

[DOI: 10.1299/mej.2014smm000x]

measured positions look elliptical particularly at $B = -90^o$ and 90^o . This represents the squareness error of B- to Z-axis average line or C- to B-axis average line. This is parameterized by α_{BY} or α_{CB} in Table 5. Note that location errors only represent the "average" error over $B = -90^o$ to 90^o. Figure 9 suggests the orientation error of the C-axis average line is larger at $B = -90^o$ and 90^o compared to that at $B = 0^o$, possibly caused by the tilt error motion (ISO 230-7, 2006) of the B-axis. Such an error motion cannot be represented by the location error; it should be parameterized by geometric error parameters that are dependent on the B-axis angular position ("position-dependent geometric errors"). The algorithm presented in Section 4.2 can be straightforwardly extended to position-dependent geometric errors, see (Ibaraki et al., 2011). For the simplicity, this paper considers only the location errors. This is why the difference between measured and simulated trajectories is larger at $B = -90^o$ and 90^o in Fig. 9.

6. Conclusion

The 5-axis continuous (scanning) on-machine geometric measurement, by using a laser displacement sensor, has a strong advantage in its measurement efficiency. In this measurement, geometric errors of rotary axes are major contributors for the measurement uncertainties.

Unlike contact-type probes, the sensor's position and orientation are calibrated in reference to the machine's motion as shown in Section 3, and thus rotary axes' geometric errors also influence them. The first contribution of this paper is on the formulation of these calibration errors.

Based on this formulation, this paper proposes an identification scheme for location errors of rotary axes, using this sensor itself. It is experimentally verified that the measuring accuracy of the sphere's displacement is sufficient to this identification method. The experimental demonstration of the identification of location errors is shown in Section 5.

References

Bringmann, B. and Knapp W., Model-based 'Chase-the-Ball' calibration of a 5-axis machining center. Annals of the CIRP, Vol. 55, No. 1 (2006), pp. 531-534.

Ibaraki, S., Oyama, C. and Otsubo, H., Construction of an error map of rotary axes on a five-axis machining center by static R-test, International Journal of Machine Tools and Manufacture, Vol. 51 (2011), pp. 190-200.

Ibaraki, S. and Ota, Y., Error Calibration for Five-Axis Machine Tools by On-the-Machine Measurement Using a Touch-Trigger Probe, International Journal of Automation Technology, Vol. 8, No. 1 (2014), pp. 20-27.

Inazaki, I., Kishinami, K., Sakamoto, S., Sugimura, N., Takeuchi, Y. and Tanaka, F., *Shaper generation theory of machine tools －its basis and applications*, Yokendo (1997), (in Japanese)

ISO 230-1:2012, Test code for machine tools －Part 1 : Geometric accuracy of machines operating under no-load or quasi-static conditions

ISO 230-7:2006, Test code for machine tools －Part 7 : Geometric accuracy of axes of rotation.

Kimura, Y., Nagai, Y. and Ibaraki, S., On-machine Measurement Using Laser Displacement Sensor under Simultaneous Five-axis Control of Target Position and Orientation, the 55th Japan Joint Automatic Control Conference (2012)

Kimura, Y., Matsubara, A. and Koike, Y., Analysis of Measurement Errors of a Diffuse-Reflection-Type Laser Displacement Sensor for Profile Measurement, International Journal of Automation Technology, Vol. 6, No. 6 (2012), pp. 724-727.

Weikert, S., R-test; a new device for accuracy measurements on five axis machine tools, Annals of the CIRP, Vol. 53, No. 1 (2004), pp. 429–32.

[DOI: 10.1299/mej.2014smm000x]